RSC Advances

PAPER

View Article Online
View Journal | View Issue

Cite this: *RSC Adv.*, 2020, **10**, 31794

Novel MoS_2 quantum dots as a highly efficient visible-light driven photocatalyst in water remediation

Linjer Chen,[a] Shu-Ling Hsieh,[b] Chia-Hung Kuo,[b] Shuchen Hsieh,[c] Wei-Hsiang Chen,[d] Chiu-Wen Chen*[a] and Cheng-Di Dong*[a]

Received 21st May 2020
Accepted 27th July 2020

DOI: 10.1039/d0ra04512h

rsc.li/rsc-advances

A direct and efficient hydrothermal system has been established for the synthesis of MoS_2 quantum dots (QDs). Novel MoS_2 QDs are an excellent potential photocatalysts to enhance photocatalytic response by charge separation under visible light irradiation. The optimum capability of QDs demonstrated the excellent photocatalytic ability for the degradation of organic pollutants. The microstructural, morphological, and optical properties of the MoS_2 QDs are defined *via* X-ray diffraction (XRD), SEM, HRTEM, XPS, and UV-Vis absorption spectroscopy techniques. Under visible light irradiation, MoS_2 QDs have great photocatalytic response for the degradation of Rh B that is 20 times higher than those of bulk MoS_2 materials. The QDs possess practically the same catalytic response after 5 recycle runs, which is an evident proof of its stability. This course might pave the route toward creating current visible-light caused QD photocatalyst strategies for the highly valuable degradation of organic pollutants or antibiotics.

Numerous methods have been employed to tackle water pollution such as physical approach, electrochemical process, adsorption with filtration path, and photodegradation routes *via* semiconductor photocatalysts.[1–4] Photocatalysis is a potential method with low power consumption; moreover, the process eliminates secondary pollution, making it an environmental-friendly and advanced pathway for the degradation of organic matter.[5–9] Even though traditional photocatalysts such as TiO_2 and ZnO have been extensively adopted, they have limitations under visible light irradiation owing to their wide bandgaps (3.2 eV) and can only absorb 5% of the UV-visible light emission.[10,11] Among the various mechanism for decontaminating water, advanced oxidation processes (AOPs) are of major research concern in recent terms. Typically, excessive oxidation potential reactive radicals (such as $HO^{\bullet}$ and $O_2^{\bullet-}$) were achieved in aqueous solutions under visible light irradiation using suitable semiconductor nanocatalysts for the elimination of the organic pollutants from essential environment. Numerous molybdenum disulfide (MoS_2)-based catalysts have been applied in numerous fields, such as photovoltaics, photocatalysis, sensors, biomedical systems, and environmental remediation owing to their great chemical stability, non-harmful, availability and equal redox potential of developed electron–hole pairs.[12,13] Lately, various shapes of nanostructures of MoS_2 were proposed as a modern type of photocatalyst for visible-light stimulated applications. There are numerous traditional approaches for MoS_2-based photocatalysts, such as hydrothermal and solid phase reaction.[14,15] These methods are successfully applied to eliminate many harmful and pollutants in aqueous solutions to acceptable degrees without reproducing further hazardous by-products.

Quantum dots (QDs) have newly been attracting wide interest as zero-dimensional nanostructures because of their low harmful, outstanding chemical stability, excellent water solubility, significant electrical conductivity, efficient degradation and photostability, and simple functionalization.[16,17] Now, QDs have been demonstrated as photocatalysts for the degradation of organic compounds owing to their reinforced properties in photocatalytic applications.[18,19] Among developed nanophotocatalysts, MoS_2 QDs have been extensively explored owing to their interesting characteristics, such as great photo stability and low band gap potential (E_g = 2.6 eV), which have performed photodegradation under sunlight or visible light. These novel QDs were accepted as unique nanophotocatalysts with high photocatalytic efficiency for the complete degradation of MB, CR, Rh B and TC in aqueous media. Previously published studies have reported that MoS_2 alone has low conductivity toward the photocatalytic field owing to the poor conductivity of MoS_2 and also due to the poor charge-carrier density. Thus,

[a]*Department of Marine Environmental Engineering, National Kaohsiung University of Science and Technology, Taiwan. E-mail: cwchen@nkust.edu.tw; cddong@nkust.edu.tw*

[b]*Department of Seafood Science, National Kaohsiung Marine University, Kaohsiung 81157, Taiwan*

[c]*Department of Chemistry and Center for Nanoscience and Nanotechnology, National Sun Yat-sen University, 70 Lien-Hai Rd, Kaohsiung 80424, Taiwan*

[d]*Institute of Environmental Engineering, National Sun Yat-sen University, Kaohsiung 804, Taiwan*

MoS_2 QDs with several nanometers in diameter and large surface area are developing into further and could be utilized for photocatalytic applications due to their quantum size effect, and the unique properties of QDs varied compared with the bulk MoS_2 or $MoSe_2$ materials. According to our results, it is possible to achieve enhanced photocatalytic reaction expected to significant response of the interfacial charge transfer. In the present work, we figure out the visible-light photocatalytic efficiency of QDs with high visible-light absorption as the environmentally beneficial, highly efficiency towards charge separation by 20-fold of the commercial bulk MoS_2 or $MoSe_2$ photocatalyst for the photodegradation of organic pollutants. In general, novel QD photocatalysts suggest better redox capability for effective charge separation due to the reduced recombination compared with the traditional photocatalysts. The QDs exhibits much higher photocatalytic performance for degrading organic pollutants and stronger photo-response than bulk MoS_2 or $MoSe_2$ alone by visible light. Therefore, we have been demonstrated that are focused on the evolution of a MoS_2-based QD photocatalyst to have potential for coming a better extent material toward capability photodegradation.

The preparation of MoS_2 QDs *via* a conventional hydrothermal route. Briefly, sodium dihydromyldimolate ($Na_2MoO_4 \cdot 2H_2O$; 1.2 mmol) was added to 20 mL of deionized water and stirred vigorously (30 min) to produce a homogeneous suspension. Then, L-cysteine ($C_3H_7NO_2S$; 2.4 mmol) was added to 20 mL of deionized water under magnetic stirring for 30 min. Further, 0.3 mL of hydrochloric acid dropwise was added to the above mixture. Later, the above two resulting mixed solutions were added to a 50 mL Teflon-lined steel autoclave, which was heated at 200 °C for 16 h. After cooling, the samples were taken and analyzed periodically each 5 min and centrifuged at a speed of 12 000 rpm min^{-1} for 10 min. Finally, the solution containing MoS_2 QDs was collected by filtering the reaction solution using a 0.22 μm syringe filter. Certainly, the as-collected QDs were dried under vacuum at 70 °C overnight for further purpose. The photocatalytic activity of the samples was investigated by monitoring the photodegradation of rhodamine B (Rh B, 3.0 mg L^{-1}, 50 mL), methylene blue (MB, 3.0 mg L^{-1}, 50 mL), a Congo red solution (CR, 3.0 mg L^{-1}, 50 mL) and tetracycline hydrochloride (TC, 10.0 mg L^{-1}, 50 mL) under visible-light illumination using a 300 W tungsten halogen lamp. In a normal photocatalytic degradation process, 3 mg of catalyst is included to 50 mL of Rh B or CR or MB or TC solution. The suspensions were magnetically stirred in dark for 90 min before visible-light irradiation. The reaction suspensions were examined at set time intervals during the photocatalysis process. The Rh B or CR or MB or TC solution was measured using a UV-Vis spectrophotometer and total organic carbon (TOC) after centrifugation.

The UV-Vis spectra of the bulk, micro-scale and MoS_2 QDs (Fig. 1(a)) indicated distinct absorption in the range of 360–450 nm owing to the excitation of electrons from the valence band to the conduction band. The absorption onset of MoS_2 is detected at approximately 400 nm. In contrast with the bulk, the micro-scale MoS_2 sample exhibits enhanced intensity of absorption in the visible range, followed by improvement in the

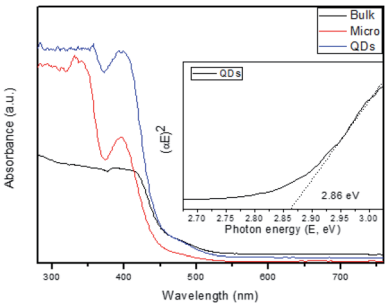

Fig. 1 The UV-Vis spectra of the bulk, micro-scale and MoS_2 QDs. The inset shows the corresponding plots of $(\alpha h\nu)^2$ against photon energy ($h\nu$).

absorption threshold owing to the quantum confinement effect.[20] These results indicate that MoS_2 QDs could be utilized as a visible-light photocatalyst. Tauc's plot (Fig. 1 inset) was employed to measure the direct band gaps of the MoS_2 QDs and found to be 2.86 eV. The band gap of pristine MoS_2 is also determined from the Tauc's plot and found to be 1.81 eV.[21] It is obvious that the bulk structure appeared with the decrease in the effective band gap owing to the promising efficient visible-light absorption and hence increasing photocatalytic efficiency.

The XPS spectroscopy was performed to check the surface chemical composition of the MoS_2 QDs. The survey spectrum

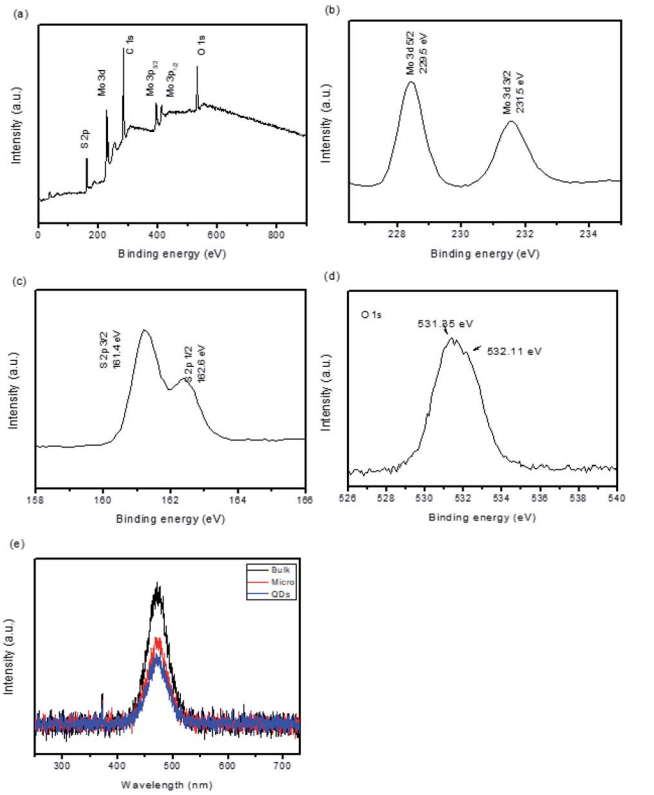

Fig. 2 The XPS spectrum of MoS_2 QDs. (a) Survey spectrum; (b) high resolution of Mo; (c) high resolution of S; (d) high resolution of O; (e) Photoluminescence spectra of prepared the bulk, micro-scale and MoS_2 QDs under 355 nm excitation.

(Fig. 2(a)) demonstrates the existence of Mo and S in atomic ratios of 22.34% and 51.48%, respectively, confirming the composition of the component. The high resolution XPS spectra of Mo (Fig. 2(b)) present two peaks. The binding energies of Mo $3d_{5/2}$ and Mo $3p_{3/2}$ are observed at 229.5 eV and 395.7 eV, respectively, which are due to the characteristic feature of MoS_2.[22] The high resolution XPS of S (Fig. 2(c)) displayed characteristic peaks with binding energy at 162.4 eV comparable to that of S $2p_{3/2}$. The peak binding energy of 531.35 and 532.11 eV are attributed to O 1s (Fig. 2d). The recombination rate of photogenerated electron–hole pairs can be explored from the PL quenching effect.[23] Fig. 2(e) demonstrates the PL spectra of the bulk, micro-scale and MoS_2 QDs at an excitation wavelength of 355 nm. It is obvious that the PL intensity comparable to the emission peak at 460 nm decreases from bulk, micro-scale and MoS_2 QDs. However, the PL emission peak intensity of MoS_2 QDs is constructed to be reduced gradually compared to the bulk and micro-scale MoS_2. This result assumed that the MoS_2 QD catalyst possesses a diminished recombination rate of photo-induced charge carriers than the bulk and micro-scale MoS_2; hence, MoS_2 QDs can hinder the exciton recombination to a better domain, thereby increasing photocatalytic performance.

The phase and crystal structures of the bulk, micro-scale and MoS_2 quantum dots were studied *via* X-ray diffraction (XRD). The XRD patterns of the bulk and micro-scale MoS_2 (Fig. 3(a) and (b)) showed indexed peaks of 14.34°, 39.56°, 44.23°, 49.86 and 60.2°, corresponding to Bragg reflections (002), (103), (006), (105) and (110) planes of MoS_2 (JCPDS Card no. 75-1539). Moreover, the diffraction peaks of the MoS_2 QDs (Fig. 3(c)) are noted at angles $2\theta = 14.21°$, 32.14° and 57.62°, corresponding to the (002), (100) and (110) lattice planes of MoS_2 (ICDD card no. 77-1716).[24] The low intensity of the diffraction peak adopted at these angles implies that the as-prepared MoS_2 has a monolayer or extremely few layers. The XRD results verify the purity of both the pristine and composite MoS_2 QDs. The morphologies of the micro-scale MoS_2 and QDs were investigated *via* TEM, and the results are exhibited in Fig. 3(d and e). From the HRTEM micrograph (Fig. 3(e)), the smaller diameters of the MoS_2 QDs were noticed to be in the range of 3.5 ± 0.5 nm. The inter planar distance was assumed to be ~0.35 nm, which corresponds to the (002) plane of hexagonal MoS_2. The SAED pattern (Fig. 3(e) inset) was established with concentric rings pointing out the high quality of crystallinity of the sample. Individual lattice planes were established and found to be consistent with the XRD pattern (Fig. 3(a)).

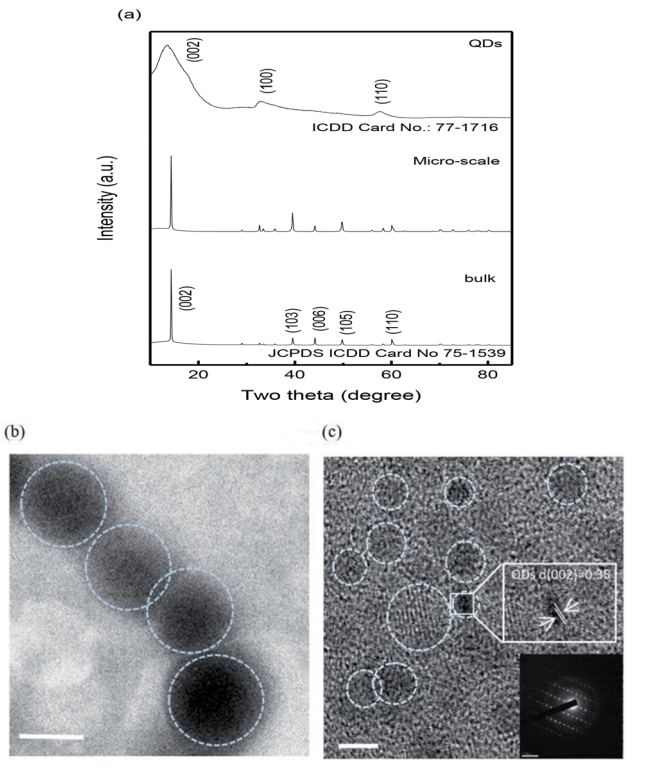

Fig. 3 (a) XRD patterns of the bulk, micro-scale and MoS_2 quantum dots. (b) TEM images of the as-prepared micro-scale MoS_2 (scale bar = 200 nm), (c) high resolution images of MoS_2 QDs (scale bar = 5 nm), the inset shows the SAED of the selected area.

We checked the visible-light-driven photocatalytic performance of the as-prepared samples using Rh B as target pollutants (Fig. 4(a)). Before the photocatalytic reaction was achieved, the adsorption–desorption behavior reached equilibrium after 10 min were organized. Bulk and micro-scale MoS_2 exhibited a rather low activity (68% and 88%) after irradiation for 60 min. However, after the diameter reduced to quantum scale, the photocatalytic performance of MoS_2 QDs clearly increased, and the MoS_2 QD photocatalyst exhibited the highest efficiency (98%) among all the samples after irradiation for 20 min. The pollutant degradation under the same conditions certainly confirmed that the MoS_2 QDs reveals enhanced photocatalytic efficiency than that of bulk and micro-scale case. When QDs are compared with all other bulk catalysts, they showed nearly the highest degradation percentage than all of the other semiconductor materials.[14,16,17] The total reaction between the QD photocatalyst and the active pollutant could be composed as supports.

$$h\nu + MoS_2QDs \rightarrow (e^-)(CB) + (h^+)(VB) \quad (1)$$

$$O_2 + (e^-)(CB) \rightarrow O_2^{\bullet -} \quad (2)$$

$$(h^+)(VB) + dye \rightarrow dye^{\bullet +} \text{ (oxidation of the pollutants)} \quad (3)$$

$$H_2O \text{ or } OH^- + (h^+)(VB) \rightarrow OH^{\bullet} \quad (4)$$

$$Dye + O_2^{\bullet -} \text{ or } OH\bullet \rightarrow \text{pollutant degradation} \quad (5)$$

The apparent rate constant (k, min^{-1}) for the degradation of Rh B can be figured out from the regression curves of $\ln(C/C_0)$ *versus* irradiation time, linearly adjusting to the pseudo first order kinetics (Fig. 4(b)). As a result, an apparent rate constant of 2.6×10^{-1} min^{-1} for MoS_2 QDs was achieved, which is remarkably higher than that of the received from its bulk and micro-scale MoS_2 (1.2×10^{-2} min^{-1} and 2.4×10^{-2} min^{-1}). The photocatalytic degradation of Rh B under visible light

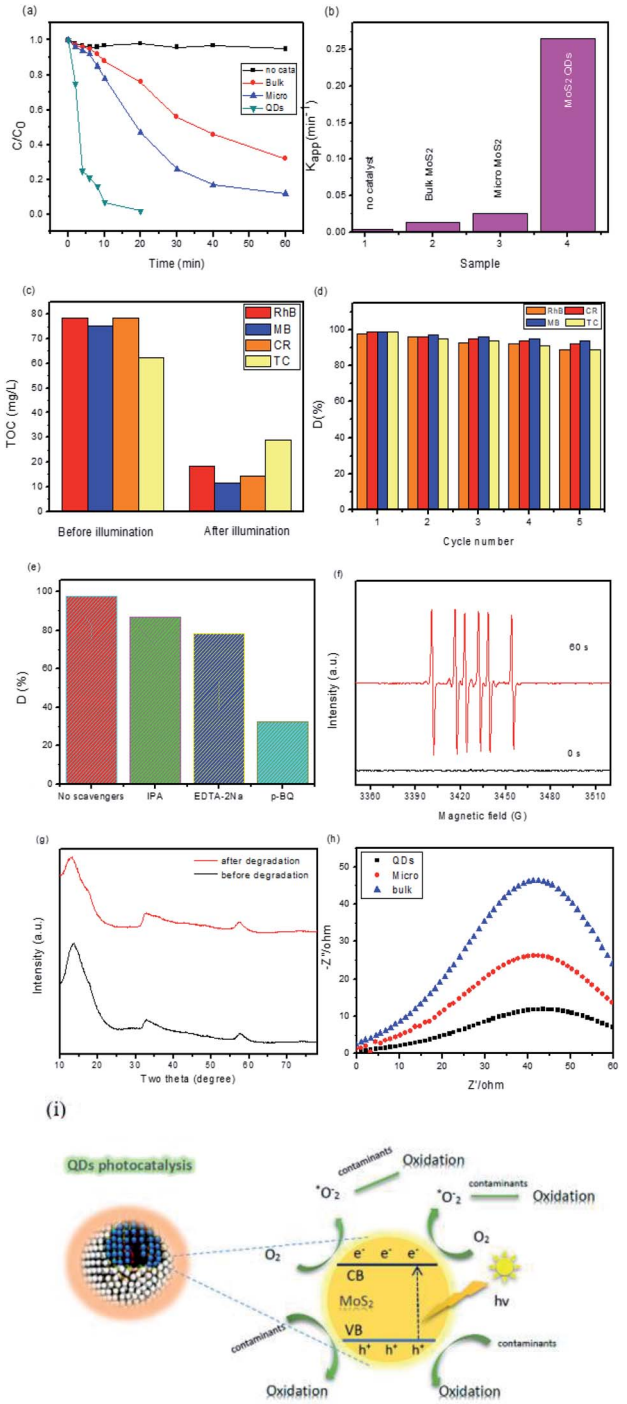

Fig. 4 (a) Photocatalytic degradation of RhB over the bulk, micro-scale and MoS_2 quantum dots under visible light irradiation, (b) comparison of apparent rate constants, (c) the TOC amount of organic pollutants before and after irradiation, (d) recycling performance of MoS_2 QDs for organic pollutants, (d) recycling performance of MoS_2 QDs for organic pollutants, (e) effect of trapping reactive species on the photocatalytic degradation pathway, (f) EPR spectra in the methanol dispersion for DMPO$^{\bullet}O_2^-$, (g) XRD pattern of the QDs before and after the photocatalytic experiment, (h) electrochemical impedance spectra, (i) the photocatalytic reaction mechanism of organic pollutants over QDs.

irradiation of the MoS_2 QDs may be due to their stronger absorption compared with that of bulk and micro-scale MoS_2. Thus, MoS_2 QDs are able to absorb a higher amount of visible light to further enhance the photocatalytic process. In addition, the better photocatalytic efficiency of MoS_2 QDs may also be due to the quantum confinement effect.[25,26] The quantum scale in the photocatalyst structure may also reduce the (e^-–h^+) pair recombination, promoting the degradation route and raising the photocatalytic activity. The apparent rate constant of MoS_2 QDs was one order of magnitude higher than that of the bulk and micro-scale MoS_2 samples, which is 20 and 10 times, respectively. The size-dependent investigation indicated that it is obvious that the degradation rate is remarkably high. The total organic carbon (TOC) experiments indicated that the TOC value was definitely decreasing (Fig. 4(c)). The removal capability of RhB, MB, CR and TC reached to 76.6%, 84.7%, 81.5% and 54.8%, respectively, which suggested that the compound was approximately degraded and no significant amount of organic species remained in the solution at the end of the degradation process. To examine the reusability of MoS_2 QDs in divided experiments, 3 mg L^{-1} of MoS_2 QDs was employed for the degradation of Rh B, MB, CR and TC (20.0 mg L^{-1} of each dye) at pH 7. In each experiment, after complete degradation, the MoS_2 QDs were separated and reused again under the same conditions. Results reported that the MoS_2 QDs exhibited an excellent stability and could be reused even after 5 rounds for Rh B, MB, CR and TC, respectively (Fig. 4(d)). The catalyst showed good recyclability up to five consecutive runs of regeneration and reuse. To further understand the photocatalysis process, trapping analyses of the active species were carried out during the photocatalytic degradation of RhB. As indicated in Fig. 4(e), for QDs, the photocatalytic degradation of RhB presents no noticeable change with isopropanol (IPA, 1 mmol L^{-1}, quencher of $^{\bullet}OH$) compared with no quencher, which suggests that $^{\bullet}OH$ is not the primary active species. When ethylenediamintetraacetic acid disodium (EDTA–2Na, 1 mmol L^{-1}, quencher of h^+) was included in the solution, the degradation of RhB slowed down slightly but was completed at about 60 min, which implies that the photogenerated holes play a minor role in the photocatalytic process. In comparison, supplement of 1, 4-benzoquinone (BQ, 0.1 mmol L^{-1}, quencher of $^{\bullet}O_2^-$) led to the complete quenching of photodegradation, suggesting that $^{\bullet}O_2^-$ is the primary active species and plays a major role in the photocatalytic process. Thus, it is apparent that $^{\bullet}O_2^-$ from the reaction of photogenerated electrons and O_2 are the essential oxidative species, while the photogenerated h^+ also supports the absolute term for the degradation of RhB in the QDs photocatalyst system. In addition, to demonstrate the active species generated in the scheme, an electron paramagnetic resonance (EPR) system was implemented to notice the generated radicals in the photocatalytic process under visible light irradiation using 5,5-dimethyl-1-pyrroline *N*-oxide (DMPO) as the radical trapping agent (Fig. 4(f)), which can trap the $^{\bullet}O_2^-$ radicals and form DMPO$^{\bullet}O_2^-$ complexes. It is established that DMPO is commonly employed as a radical trapping agent, forming DMPO–$^{\bullet}O_2^-$. Briefly, 5 mg of the QDs catalyst was dispersed in methanol (for $^{\bullet}O_2^-$) and thus DMPO (20 mM) was included with ultrasonic dispersion for 5 min. The signal intensity is continuously raised with increasing irradiation time. The component peaks of DMPO$^{\bullet}O_2^-$ can be detected in the methanol dispersion

of QDs after visible light irradiation, implying that the $^{\bullet}O_2^-$ radicals were developed from the reaction of photogenerated electrons and O_2 molecules in the photocatalytic processes. Associated with the trapping analyze, it can be assumed that $^{\bullet}O_2^-$ played a crucial role in the photocatalytic process. These results suggest that $^{\bullet}O_2^-$ is the primary active species and the principal mechanism for the great photocatalytic action, supported by h^+, whereas $^{\bullet}OH^-$ showed only a rather trivial role in the whole photocatalytic process. In addition, XRD patterns were employed to determine the crystal structure of the MoS_2 QDs before and after the photocatalytic degradation route of RhB as indicated in Fig. 4(g). No other impurity diffraction peaks after five continuing cycles were detected, and the crystal phase is stable after the degradation process. It is noted that the intensities of the primary peaks are broad and weak, which suggest that the crystallinity is weak and the crystallite size is limited. The electron hole-pair separation plays an important part in increasing the photocatalytic activity. This can clearly be measured by performing the electrochemical impedance spectroscopy (EIS) of the concerned semiconductor process. Fig. 4(h) shows the Nyquist plots of the bulk, micro-scale and MoS_2 QDs. The curves for each photocatalysts are the combination of three distinct semicircles in higher and lower frequency fields. Typically, the smaller arc radius denotes the efficient charge transfer at the interface. Herein, the arc radius of MoS_2 QDs was noticed to be the smallest of all, which indicates that MoS_2 QDs receive the highest rate of electron transport and lowest rate of electron hole pair recombination. The following is also in accordance with the clearly increased photocatalytic activity of the MoS_2 QD sample. However, the weaker PL intensity of MoS_2 QDs (Fig. 2(e)) suggests a lower recombination rate of photogenerated electrons and holes. In addition, related to bulk and micro-scale MoS_2 show advantages such as a greater specific surface area, a slightly greater oxidizing capability, and a higher internal electric field, which are favorable for photocatalysis.[27] A feasible photocatalytic degradation mechanism is illustrated in Fig. 4(i). Thus, the photogenerated electrons located on MoS_2 QDs with strong reduction capacity can more easily move to the surface active positions, leading a capable photocatalytic redox reaction.

Conclusions

In summary, MoS_2 QD photocatalysts have been well performed and developed through the combination of hydrothermal systems. The QDs degraded 98% of the cationic dye (RhB) in 20 min of visible light irradiation at a rate constant 2.6×10^{-2} min^{-1}. A 20-fold increment (one order of magnitude) in the photocatalytic activity as compared to bulk MoS_2 has been achieved due to better charge separation of electron–hole pairs in the QD system. Photocatalytic stability analyses conducted on the MoS_2 QDs exhibited excellent stability and the degradation percentage ranged from 98% to 90% after 5 consecutive degradation cycles. The trapping experiments demonstrated that $^{\bullet}O_2^-$ (superoxide radical) were the primary active species for organic pollutants degradation. This work has been demonstrated that this QDs photocatalytic pathway will suggest new designs for resolving deficient photocatalytic behavior and obtaining further aspect in potential improvement and environmental protection.

Conflicts of interest

There are no conflicts to declare.

Notes and references

1 M. Pálmai, E. M. Zahran, S. Angaramo, S. Bálint, Z. Pászti, M. R. Knecht and L. G. Bachas, Pd-decorated m-$BiVO_4$/BiOBr ternary composite with dual heterojunction for enhanced photocatalytic activity, *J. Mater. Chem. A*, 2017, **5**, 529–534.

2 S. Dong, X. Ding, T. Guo, X. Yue, X. Han and J. Sun, Self-assembled hollow sphere shaped Bi_2WO_6/RGO composites for efficient sunlight-driven photocatalytic degradation of organic pollutants, *Chem. Eng. J.*, 2017, **316**, 778–789.

3 S. Dong, L. Cui, C. Liu, F. Zhang, K. Li, L. Xia, X. Su, J. Feng, Y. Zhu and J. Sun, Fabrication of 3D ultra-light graphene aerogel/Bi_2 WO_6 composite with excellent photocatalytic performance: A promising photocatalysts for water purification, *J. Taiwan Inst. Chem. Eng.*, 2019, **97**, 288–296.

4 D. Wu, R. Wang, C. Yang, Y. An, H. Lu, H. Wang, K. Cao, Z. Gao, W. Zhang, F. Xu and K. Jiang, Br doped porous bismuth oxychloride micro-sheets with rich oxygen vacancies and dominating {0 0 1} facets for enhanced nitrogen photo-fixation performances, *J. Colloid Interface Sci.*, 2019, **556**, 111–119.

5 Y. Cho, S. Shoji, A. Yamaguchi, T. Hoshina, T. Fujita, H. Abe and M. Miyauchi, Visible-light-driven dry reforming of methane using semiconductor-supported catalyst, *Chem. Commun.*, 2020, **56**, 4611–4614.

6 F. Pang, Y. Jiang, Y. Zhang, M. Y. He and J. Ge, Synergetic enhancement of photocatalytic activity with a photonic crystal film as a catalyst support, *J. Mater. Chem. A*, 2015, **3**(43), 21439.

7 S. Dong, L. Xia, T. Guo, F. Zhang, L. Cui, X. Su, D. Wang, W. Guo and J. Sun, Controlled synthesis of flexible graphene aerogels macroscopic monolith as versatile agents for wastewater treatment, *Appl. Surf. Sci.*, 2018, **445**, 30–38.

8 L. Tan, C. Yu, M. Wang, S. Zhang, J. Sun, S. Dong and J. Sun, Synergistic effect of adsorption and photocatalysis of 3D g-C_3N_4-agar hybrid Aerogels, *Appl. Surf. Sci.*, 2019, **467–468**, 286–292.

9 S. Dong, L. Cui, W. Zhang, L. Xia, S. Zhou, C. K. Russell, M. Fan, J. Feng and J. Sun, Double-shelled $ZnSnO_3$ hollow cubes for efficient photocatalytic degradation of antibiotic wastewater, *Chem. Eng. J.*, 2020, **384**, 123279.

10 A. M. Lacerda, I. Larrosa and S. Dunn, Plasmon enhanced visible light photocatalysis for TiO_2 supported Pd nanoparticles, *Nanoscale*, 2015, **7**, 12331–12335.

11 D. Wu, X. Wang, H. Wang, F. Wang, D. Wang, Z. Gao, F. Xu and K. Jiang, Ultrasonic-assisted synthesis of two dimensional BiOCl/MoS_2 with tunable band gap and fast

charge separation for enhanced photocatalytic performance under visible light, *J. Colloid Interface Sci.*, 2019, **533**, 539–547.

12 S. Chandrasekaran, L. Yao, L. Deng, C. Bowen, Y. Zhang, S. Chen, Z. Lin, F. Peng and P. Zhang, Recent advances in metal sulfides: from controlled fabrication to electrocatalytic, photocatalytic and photoelectrochemical water splitting and beyond, *Chem. Soc. Rev.*, 2019, **48**, 4178–4280.

13 J. Chen, D. Wu, H. Wang, F. Wang, Y. Wang, Z. Gao, F. Xu and K. Jiang, In-situ synthesis of Molybdenum Sulfide/Reduced Graphene Oxide porous film as robust counter electrode for dye-sensitized solar cells, *J. Colloid Interface Sci.*, 2018, **524**, 475–482.

14 W. Gao, M. Wang, C. Ran and Li Le, Facile one-pot synthesis of MoS_2 quantum dots/Graphene/TiO_2 composites for highly enhanced photocatalytic property, *Chem. Commun.*, 2015, **51**, 1709–1712.

15 L. Wang, D. Wu, Z. Guo, J. Yan, Y. Hu, Z. Chang, Q. Yuan, H. Ming and J. Wang, Ultra-thin TiO_2 sheets with rich surface disorders for enhanced photocatalytic performance under simulated sunlight, *J. Alloys Compd.*, 2018, **745**, 26–32.

16 R. Shi, F. Liu, Z. Wang, Y. Weng and Y. Chen, Black/red phosphorus quantum dots for photocatalytic water splitting: from a type I heterostructure to a Z-scheme system, *Chem. Commun.*, 2019, **55**, 12531.

17 D. Wu, Y. Wang, F. Wang, H. Wang, Y. An, Z. Gao, F. Xu and K. Jiang, Oxygen-incorporated few-layer MoS2 vertically aligned on three dimensional graphene matrix for enhanced catalytic performances in quantum dot sensitized solar cells, *Carbon*, 2017, **123**, 756–766.

18 B. Bajorowicz, E. Kowalska, J. Nadolna, Z. Wei, M. Endo, B. Ohtani and A. Zaleska-Medynska, Preparation of CdS and Bi_2S_3 quantum dots co-decorated perovskite-type $KNbO_3$ ternary heterostructure with improved visible light photocatalytic activity and stability for phenol degradation, *Dalton Trans.*, 2018, **47**, 15232–15245.

19 K. Bhuvaneswari, V. Vaitheeswari, G. Palanisamy, T. Maiyalagan and T. Pazhanivel, Glutathione capped inverted core-shell quantum dots as an efficient photocatalyst for degradation of organic dyes, *Mater. Sci. Semicond. Process.*, 2020, **106**, 104760.

20 A. P. Manuel, A. Kirkey, N. Mahdi and K. Shankar, Plexcitonics – fundamental principles and optoelectronic applications, *J. Mater. Chem. C*, 2019, **7**, 1821–1853.

21 X. Wang, G. Sun, N. Li and P. Chen, Quantum dots derived from two-dimensional materials and their applications for catalysis and energy, *Chem. Soc. Rev.*, 2016, **45**, 2239–2262.

22 H. W. Wang, P. Skeldon and G. E. Thompson, XPS studies of MoS_2 formation from ammonium tetrathiomolybdate solutions, *Surf. Coat. Technol.*, 1997, **91**, 200–207.

23 V. G. Deonikar, S. S. Patil, M. S. Tamboli, J. D. Ambekar, M. V. Kulkarni, R. P. Panmand, G. G. Umarji, M. D. Shinde, S. B. Rane, N. R. Munirathnam, D. R. Patil and B. B. Kale, Growth study of hierarchical Ag_3PO_4/$LaCO_3OH$ heterostructures and their efficient photocatalytic activity for RhB degradation, *Phys. Chem. Chem. Phys.*, 2017, **19**, 20541–20550.

24 S. Hariharan and B. Karthikeyan, Optical and surface band bending mediated fluorescence sensing properties of MoS_2 quantum dots, *RSC Adv.*, 2016, **6**, 101770–101777.

25 P. Dong, G. Hou, X. Xi, R. Shao and F. Dong, WO_3-based photocatalysts: morphology control, activity enhancement and multifunctional applications, *Environ. Sci.: Nano*, 2017, **4**, 539–557.

26 C. Xu, P. R. Anusuyadevi and C. Aymonier, Rafael Luque and Samuel Marre, Nanostructured materials for photocatalysis, *Chem. Soc. Rev.*, 2019, **48**, 3868–3902.

27 Z. Gao and X. Qu, Construction of $ZnTiO_3$/Bi_4NbO_8Cl heterojunction with enhanced photocatalytic performance, *Nanoscale Res. Lett.*, 2020, **15**, 64.